

Supplementary information for *Through-thickness resolution, stress oscillations and residual stress in cold rolling*

1. ABAQUS formulation

We present here some relevant background information on the FE modelling technique for rolling. The metal rolling process is governed by differential equations describing yield conditions, constitutive relationships and conservation of mass and momentum. In FE analysis, the differential equations are approximately solved between a discrete set of nodes, using shape functions that assume a particular interpolation field between the nodes. This approach discretises spatial derivatives, so that the partial differential equations are transformed into a system of ordinary differential equations. The simplified form of the equations of motion are written as

$$\mathbf{M}\ddot{\mathbf{u}} = \mathbf{f}^{\text{ext}} - \mathbf{f}^{\text{int}}, \quad (1)$$

where \mathbf{M} is the diagonal mass matrix, \mathbf{u} is the nodal displacement vector, and \mathbf{f}^{ext} and \mathbf{f}^{int} are the external and internal nodal force vectors respectively [1]. In modelling of metal sheet rolling, inertia effects are often neglected [2–4].

FE simulations reported in this work were conducted using ABAQUS 2021 [5]. Within ABAQUS there are two numerical formulations: implicit and explicit. We give a brief overview of each formulation before discussing their relative merits for the problem of interest.

1.1. ABAQUS/Standard formulation

ABAQUS/Standard is an implicit solver where the model is updated from time t to time $t + \Delta t$ using information from times t and $t + \Delta t$. In this work, only static analyses are considered in ABAQUS/Standard. Therefore, since inertia is ignored, the relevant equations of motion are

$$\mathbf{F}(\mathbf{u}) = \mathbf{f}^{\text{ext}} - \mathbf{f}^{\text{int}} = \mathbf{0}. \quad (2)$$

This large system of equations is solved iteratively in each time increment to obtain the updated nodal displacements, using the Newton–Raphson technique. The displacements are updated via

$$\Delta \mathbf{u}_{(n+1)}^{(t+\Delta t)} = \left[\mathbf{K}_{(n)}^{(t+\Delta t)} \right]^{-1} \cdot \left(\mathbf{F}_{(n)}^{(t+\Delta t)} \right), \quad (3a)$$

$$\mathbf{u}_{(n+1)}^{(t+\Delta t)} = \mathbf{u}_{(n)}^{(t+\Delta t)} + \Delta \mathbf{u}_{(n+1)}^{(t+\Delta t)}, \quad (3b)$$

where the superscript $(t + \Delta t)$ is the time at which the equations are evaluated, the subscripts (n) and $(n + 1)$ indicate the current and next iterations respectively and $\mathbf{K}_{(n)} = (\partial \mathbf{F} / \partial \mathbf{u})_{(n)}$ is the stiffness matrix at iteration n . The inversion of the stiffness matrix $\mathbf{K}_{(n)}$ is computationally expensive. The convergence of the Newton–Raphson method is measured by ensuring that all entries $\mathbf{F}(\mathbf{u})$ and $\Delta \mathbf{u}$ are sufficiently small [6]. At the end of time increment t , the next time increment $t + \Delta t$ is attempted, and load or displacement is incremented corresponding to Δt . If convergence is not achieved by ABAQUS in a certain time increment, Δt is reduced and the Newton–Raphson method is attempted again. The reader should note that no velocities or accelerations are given by ABAQUS/Standard for static analyses. These can be manually extracted via postprocessing of the displacements (see Section 4 for more details).

1.2. ABAQUS/Explicit formulation

In ABAQUS/Explicit, the equations are solved for future time steps using known information, making it an explicit scheme. This dynamic solution scheme necessitates the full version of equation (1) to be solved. The diagonal mass matrix is inverted to find the vector of nodal accelerations,

$$\ddot{\mathbf{u}}^{(i)} = \mathbf{M}^{-1} (\mathbf{f}^{\text{ext}} - \mathbf{f}^{\text{int}}), \quad (4)$$

at the beginning of time increment i . The inversion of the mass matrix is numerically much simpler than inverting the stiffness matrix [7]. The acceleration vector $\ddot{\mathbf{u}}^{(i)}$ is assumed to remain constant for a very small time increment and the explicit central-difference integration rule [8] is used to update the mid-increment velocities and subsequently the end-of-increment displacements,

$$\dot{\mathbf{u}}^{(i+\frac{1}{2})} = \dot{\mathbf{u}}^{(i-\frac{1}{2})} + \frac{\Delta t^{(i+1)} + \Delta t^{(i)}}{2} \ddot{\mathbf{u}}^{(i)}, \quad (5a)$$

$$\mathbf{u}^{(i+1)} = \mathbf{u}^{(i)} + \Delta t^{(i+1)} \dot{\mathbf{u}}^{(i+\frac{1}{2})}. \quad (5b)$$

The explicit dynamics procedure is ideally suited for analysing high-speed dynamic events, but many of the advantages of the explicit procedure also apply to the analysis of slower (quasi-static) processes. Quasi-static analyses typically have longer timescales which increase the numerical computation time required by FE methods. The stable time increment for ABAQUS/Explicit simulations is the largest possible time step the solver can take without results becoming unstable. When the solution becomes unstable, the time-history response of solution variables such as displacements will usually oscillate with increasing amplitudes [5]. This stability limit is also known as the Courant–Friedrich–Lewy (CFL) limit [9], and is estimated as

$$\Delta t_{\text{stable}} \approx \frac{L^e \sqrt{\rho}}{\sqrt{E}}, \quad (6)$$

where L^e is the smallest element dimension in the FE model, ρ is the material density and E is the Young’s modulus of the material. However, ABAQUS/Explicit enables the use of mass scaling. Mass scaling uniformly scales the density of the material within the simulation to facilitate longer time steps and reduce computational time [4]. The limited time increment means that explicit methods are conditionally stable, thus the mass scaling factor (MSF) must be chosen carefully to reduce simulation times without introducing inertial effects. The introduction of inertial effects can lead to erroneous and unstable outputs [1, 10, 11]. The general rule of thumb to assess inertial effects is to ensure that the ratio between the kinetic energy and the internal energy is small (5–10%) [5, 7].

1.3. General FE model conditions

Some of the FE model conditions are specific to the solver type (i.e. implicit or explicit); these are summarized in Table 1. We will compare results from four-node, plane-strain elements, specifically: for implicit analyses, full-integration (CPE4), incompatible (CPE4I) and reduced-integration (CPE4R) element types; for explicit analysis, since full-integration (CPE4) and incompatible type (CPE4I) elements are not offered by ABAQUS/Explicit, only reduced-integration (CPE4R) elements are considered.

1.4. Transient effects and job precision

Our focus in this paper is on steady-state behaviour, so we aim to minimise transient effects. Implicit simulations detailed here apply an instantaneous $\Omega = 5 \text{ rad s}^{-1}$ while explicit simulations smoothly ramp roller speed to $\Omega = 5 \text{ rad s}^{-1}$. Mass scaling and/or increased loading rates were not applied to the explicit analysis, and a smooth amplitude method was used, again to minimize transient effects. Explicit simulations were conducted using double precision for both the packager and analyses. This is equivalent to the full nodal precision requested in implicit analyses.

Feature	ABAQUS/Standard	ABAQUS/Explicit
Density	N/a	7831.3 kg m ⁻³
Step type	Static, general	Dynamic, explicit
Amplitude curve	Instantaneous	Smooth step
Contact tracking	State-based	N/a
Contact discretisation	Surface-to-surface	N/a
Mechanical constraint formulation	N/a	Kinematic contact
Element types considered	CPE4/CPE4I/CPE4R	CPE4R
ABAQUS/Explicit precision	N/a	Double, analysis & packager

Table 1: Unique FE model settings for the ABAQUS/Standard and ABAQUS/Explicit rolling models used in this work. The amplitude curve information relates to the application of loading on the roller during the rolling step, not the bite step.

1.5. Relative merits

For the cold rolling process it is not immediately clear which of the formulations outlined above is best as each type offers different advantages and disadvantages. The explicit solver is often the preferred choice for modelling metal forming processes due to its computational speed and robust handling of complex contact conditions [8, 9, 12, 13]. A key disadvantage of choosing the explicit solver is the absence of equilibrium convergence enforcement which can lead to error accumulation [14]. The potential for explicit solvers to accumulate error implies that implicit solvers provide stronger results, since convergence is ensured at each time increment in implicit analyses [15]. However, implicit solvers typically consume more computational resources and can struggle to handle complex contact [9]. In the analysis below we will assess both implicit and explicit solvers for modelling cold rolling, with the specific aim of accurately capturing through-thickness variations of stress and strain quantities.

2. FE model refinement

Here we detail our investigation of the effect of solver (i.e., implicit versus explicit) and element type through-thickness stress and strain predictions. This supplements our mesh and steady state convergence studies in the main text.

2.1. Element type

The material response is evaluated by Gaussian quadrature at each element integration point [5]. In this work, first-order plane-strain elements are employed to discretise the sheet. Other authors [12, 16–19] similarly used first-order elements to model rolling. Fully-integrated plane-strain four-node (CPE4) elements contain a total of four integration points. The number of nodes and/or number of integration points correlates to the degrees of freedom any given element can exhibit. Reduced-integration elements, such as CPE4R elements, use just a single integration point in the centre of the element (compared to the four integration points in a fully-integrated CPE4 element). Therefore, in principle, CPE4 elements are more accurate than the CPE4R elements. However, in the presence of bending moments the inherent linear geometry of CPE4 elements can give rise to large, artificial shear strains. This problematic behaviour is often termed “shear locking” [20, 21]. Shear locking is a purely computational behaviour and is not representative of physical processes. FE models exhibiting shear locking provide erroneous displacement and stress values [20]. All three element types mentioned here are available for implicit analysis in ABAQUS, while only CPE4R are available for explicit analysis.

2.1.1. Implicit analysis — three elements

Figure S1 shows a checkerboard pattern in the shear stress which is evaluated at the integration points of CPE4 elements during a rolling simulation with $N_e = 40$ elements through the half-thickness of the sheet. This checkerboard pattern is typical of shear locking behaviour [5]. Figure S2 shows a quantitative

comparison between the aforementioned CPE4 shear results and shear outputs from a simulation that employs $N_e = 40$ CPE4R elements through the half-thickness. Interpolation is carried out in the z -direction to facilitate comparison between different mesh types. The solid, dotted and dashed curves depict results in the sheet at $x = 0.025L$, $x = 0.6913L$ and $x = 1.09L$, respectively¹. Figure S2 shows sharp changes in the nodal CPE4 shear results, particularly towards the surface of the sheet (i.e., higher z/h_0 values) at $x = 0.025L$ and $x = 0.6913L$ (the solid and dotted curves respectively), highlighting the non-smooth nature of the shear results that is also visible in Figure S1. In contrast, the CPE4R results are quite smooth everywhere, confirming that shear locking is not an issue for CPE4R elements. The checkerboard pattern (Figure S1) and the interpolated shear results (Figure S2) imply that CPE4 elements are not suitable for this test case and hence this element type is not considered for the remainder of this work.

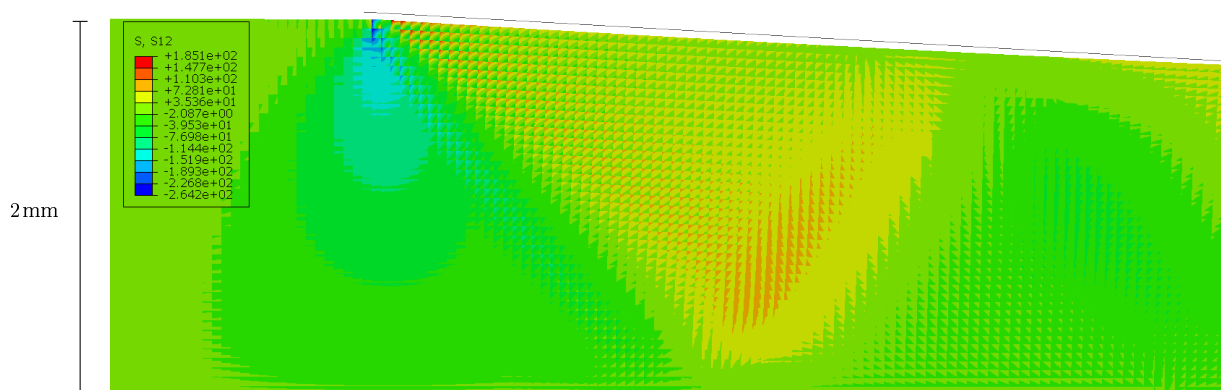


Figure S1: Shear stress (MPa) evaluated at the integration points (i.e., no nodal averaging) for a rolling simulation using $N_e = 40$ CPE4 elements through the half-thickness. Jumps in shear stress between elements create a checkerboard pattern, typical of shear-locking behaviour.

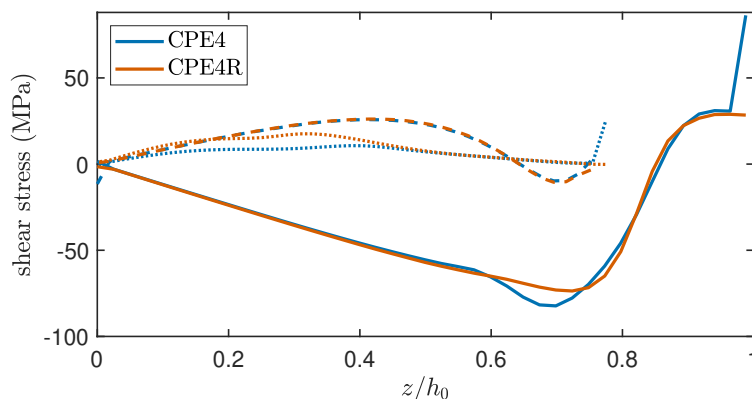


Figure S2: Interpolated shear stress (MPa) from two simulations employing $N_e = 40$ CPE4 and CPE4R elements through the half-thickness, evaluated at horizontal positions $x/L = 0.025$ (solid lines), 0.6913 (dotted lines) and 1.09 (dashed lines) and plotted as a function of vertical distance from the sheet centerline. Roller radius is $R = 257.45$ mm and roll gap aspect ratio is $1/\varepsilon = 8$.

Unlike CPE4 elements, plane-strain reduced-integration (CPE4R) and incompatible (CPE4I) elements do not suffer from shear-locking behaviour. Low-order elements such as CPE4R lack the necessary shape

¹These three x -positions represent the positions where maximum relative errors were observed in our convergence analysis (see 3 for more details)

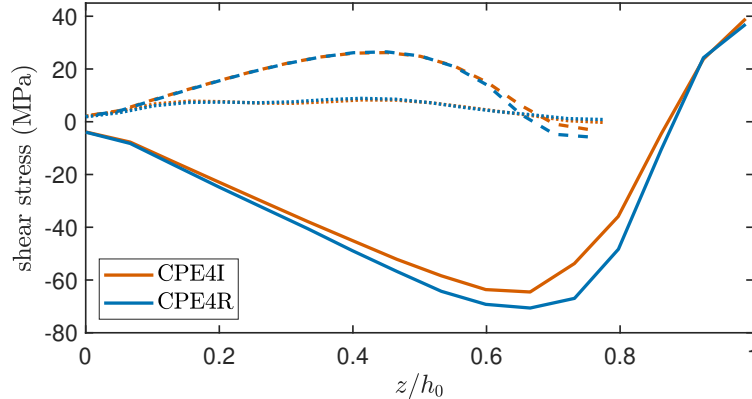


Figure S3: Interpolated shear from two simulations employing $N_e = 15$ CPE4I and CPE4R elements through the half-thickness, evaluated at horizontal positions $x/L = 0.025$ (solid lines), 0.6913 (dotted lines) and 1.09 (dashed lines) and plotted as a function of vertical distance from the sheet centerline. Roller radius is $R = 257.45$ mm and roll gap aspect ratio is $1/\varepsilon = 8$. CPU times are 17.7 hours for CPE4I and 3.2 hours for CPE4R.

functions to describe bending, while incompatible elements such as CPE4I artificially add the required shape functions to adequately describe this behaviour [22, 23]. Incompatible elements are slow to converge in simulations with large compressive strains [5]. For example, a simulation with $N_e = 15$ CPE4I elements through the half-thickness took over 5.5 times as long as a simulation with $N_e = 15$ CPE4R elements. Simulations with CPE4I and CPE4R elements give similar results (see Figure S3) and the large computational time severely restricts the mesh size that can be employed with the CPE4I element type, so CPE4I elements are not considered for the remainder of this work.

2.1.2. Hourglassing

While reduced-integration elements are often recommended as a means of mitigating shear locking [1, 22, 24], they can suffer from spurious zero-energy element deformations. These zero-energy deformations are often known as “hourglass” modes [20, 25]. ABAQUS offers controls to mitigate against this unrealistic zero-energy behaviour. The default total stiffness hourglass controls are applied to simulations in this work. Default hourglass controls apply additional stiffness to elements to counteract hourglass modes. To obtain physically reliable results, the artificial energy used to control hourglassing must be small ($<10\%$) compared to the internal energy in the model [5, 25–27]. In this work the artificial energy is less than 0.5% of the internal energy for all simulations. Given the small energy ratio and considering that hourglass behaviour is not visible in the deformed mesh of any simulation, we conclude that hourglassing does not occur in simulations reported here. Therefore CPE4R elements are the most appropriate element for this research.

2.2. Limitations of ABAQUS/Explicit

We now consider results from ABAQUS/Explicit simulations. Mass scaling (or increased loading rate) was not used in any explicit simulation in this paper. Given that the kinetic-to-internal energy ratio remains in the desired range (5–10%) [5, 7], we consider inertia effects to be insignificant.

Figures S4a and S4b compare the von Mises stress for two explicit simulations with mesh densities of $N_e = 5$ and $N_e = 40$ elements through the half-thickness, respectively. The most notable difference between the plots is the smoothness of the solution. As mesh density increases, it is expected that the calculation accuracy should, in general, improve [28]. However, Figure S4 shows that increasing the mesh density increases noise, indicating that the solution diverges as mesh density increases. In particular, we note the numerical noise near the surface of the sheet towards the entrance to the roll gap, $x/L = 0$. This noise is likely an artefact of the lack of convergence checks performed by ABAQUS/Explicit at each time increment, which allows the solution to diverge without restriction. In a recent conference paper [29], we successfully removed such noise by implementing additional stiffness-proportional damping. However, the

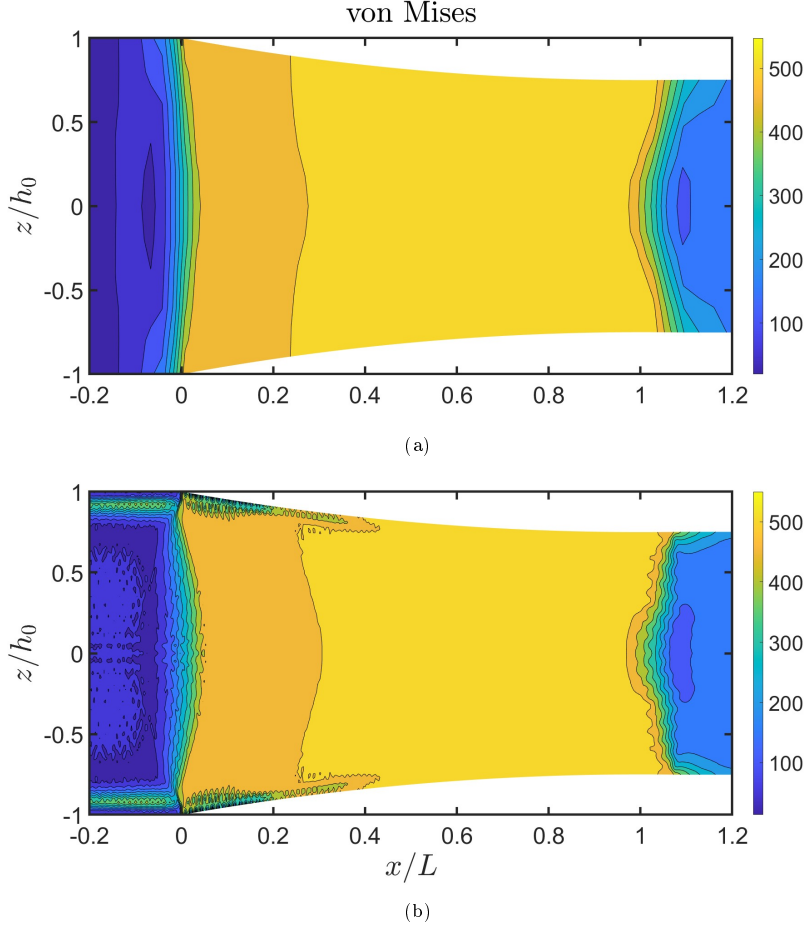


Figure S4: Contour plots showing von Mises stress (MPa) from explicit simulations with (a) $N_e = 5$ CPE4R elements and (b) $N_e = 40$ CPE4R elements, where the symmetry axis is located at $z/h_0 = 0$. Both simulations have roller radius $R = 257.45$ mm and $\varepsilon = 0.125$.

damping approach increases the required computational time (700 CPU hours compared to 10 CPU hours without damping for a particular rolling simulation conducted in [29]). Although the explicit simulations are typically quicker to execute than their implicit counterparts (for example, with $N_e = 40$ CPE4R elements through the half-thickness, the explicit simulation's CPU time is less than 37% than that of the equivalent implicit simulation), the divergent nature of the explicit results and the lack of equilibrium checks lead us to proposing that implicit simulations outperform explicit simulations for this case study. Therefore the remainder of this work will focus on simulation results from implicit simulations only.

3. Relative error: choice of x/L locations

We detail here how the three x/L positions used in the interpolated results throughout this paper were chosen. These x/L positions represent the positions of maximum relative errors. To explain how these errors are calculated, consider the plots as a function of vertical position in Figure 4 in the main text. The (interpolated) results from each simulation are interpolated onto a curve with 41 z/h_0 points, so that we can compute the absolute difference between this and the (interpolated) simulation with $N_e = 40$ elements. We then compute a relative error by dividing the absolute difference by the maximum value across the entire roll gap, as predicted by the simulation with $N_e = 40$. We choose to normalize this way as opposed to relative to the local value because some quantities go through zero. At each x/L location, the maximum

relative error value out of the 41 z/h_0 values is stored in an array and plotted in Figure S5 as a function of x/L . We considered 100 x/L positions from $x/L = 0.025$ up to $x/L = 1.25$. Note that $x/L < 0.025$ was not considered. The contact point occurs in the neighbourhood of $x/L = 0$ and corresponds to a change from zero to large normal stress, so a small change in the predicted position of the contact point can lead to misleadingly large errors recorded at $x/L = 0$.

Figure S5 shows that $x/L = 0.025$ is a position where high relative errors occur, and hence this is one of the x/L positions used for interpolations in this paper. Figure S5a and Figure S5b also show a spike in relative errors near $x/L = 1.09$. This is another x/L position used to calculate the interpolated results. It is not clear from Figure S5b and Figure S5c which third x/L position to choose. However, Figure S5a shows a small peak in relative error around the neutral point at $x/L = 0.6913$ (the neutral point value of $x/L = 0.6913$ is predicted by the implicit simulation with $N_e = 40$). Given this peak and the interesting dynamics around the neutral point in general, $x/L = 0.6913$ is the third position used in the interpolated results throughout this paper.

4. FE velocity calculation

ABAQUS/Standard does not output velocity components or PEEQ rate values for static analyses. Therefore, we manually calculate the velocity and PEEQ rate values. The velocity and PEEQ rate approximations are conducted via a Lagrangian time derivative of the displacements and the PEEQ values respectively. Since the procedure is identical for calculating both velocity and PEEQ rate values, we give details of the velocity calculation only.

All stress and strain quantities are outputted to an output database (*.ODB*) file for all ABAQUS simulations. These quantities are available at different time points throughout the simulation, and it is possible for the user to vary the number and frequency of the time points throughout each analysis step. To approximate the velocity components (v_x, v_z) of some arbitrary node in the sheet, at time frame f , we use a fourth-order-accurate central differencing operator on the displacements

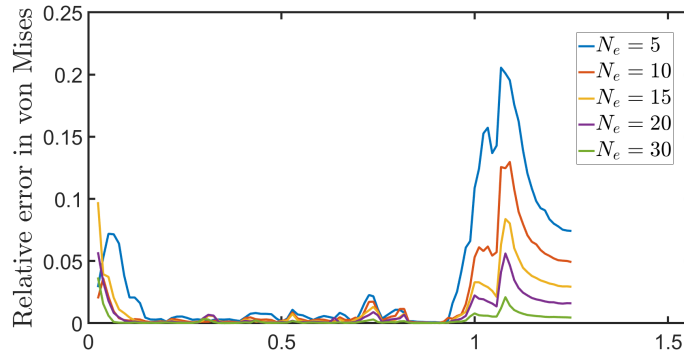
$$v_x^{(f)} = \frac{\frac{1}{12}u_x^{(f-2)} - \frac{2}{3}u_x^{(f-1)} + \frac{2}{3}u_x^{(f+1)} - \frac{1}{12}u_x^{(f+2)}}{\Delta t}, \quad (7a)$$

$$v_z^{(f)} = \frac{\frac{1}{12}u_z^{(f-2)} - \frac{2}{3}u_z^{(f-1)} + \frac{2}{3}u_z^{(f+1)} - \frac{1}{12}u_z^{(f+2)}}{\Delta t}, \quad (7b)$$

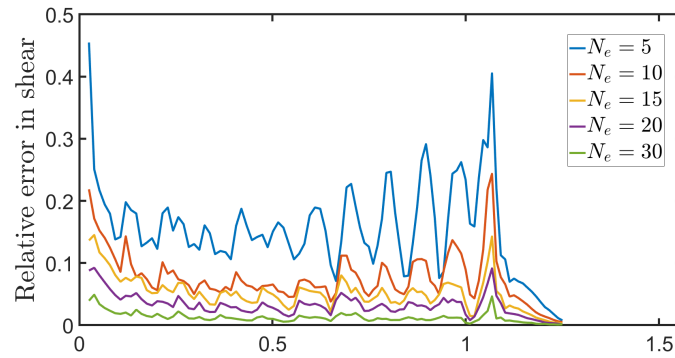
where Δt is constant between all time frames considered. In order to allow velocities and all other stress and strain components to be evaluated at the same time frame, all data in the main text is evaluated at a time point that is two time frames before $t = 0.1$ s, which is the end of the *rolling* step. The authors ensured that Δt is sufficiently small for accurate velocity approximations.

References

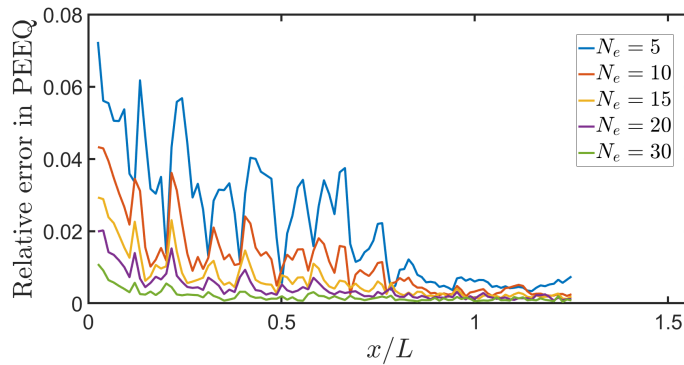
- [1] A. Hadadian, R. Sedaghati, Investigation on thermal relaxation of residual stresses induced in deep cold rolling of Ti-6Al-4V alloy, *The International Journal of Advanced Manufacturing Technology* 100 (2019) 877–893.
- [2] I. Tarnovskii, A. Pozdeyev, V. Lyashkov, *Deformation of metals during rolling* (English edition), Pergamon Press, 1965.
- [3] C. Cawthorn, J. Minton, E. Brambley, Asymptotic analysis of cold sandwich rolling, *International Journal of Mechanical Sciences* 106 (2016) 184–193.
- [4] J. Minton, *Mathematical modelling of asymmetrical metal rolling processes*, Ph.D. thesis, University of Cambridge, 2017.
- [5] Dassault Systèmes, *SIMULIA User Assistance 2021 Abaqus*, 2021.
- [6] Z. Jiang, A. Tieu, Elastic–plastic finite element method simulation of thin strip with tension in cold rolling, *Journal of Materials Processing Technology* 130 (2002) 511–515.
- [7] P. Natário, N. Silvestre, D. Camotim, Web crippling failure using quasi-static FE models, *Thin-Walled Structures* 84 (2014) 34–49.
- [8] E. Gavalas, I. Pressas, S. Papaefthymiou, Mesh sensitivity analysis on implicit and explicit method for rolling simulation, *International Journal of Structural Integrity* 9 (2018) 465–474.
- [9] N. Padhye, Mechanics and modeling of cold rolling of polymeric films at large strains—a rate-independent approach, *Mechanics of Materials* 184 (2023) 104733.



(a)



(b)



(c)

Figure S5: Relative error in (a) von Mises stress, (b) shear stress and (c) PEEQ (plastic equivalent strain) from simulations with varying mesh densities. All simulations are compared to a simulation with $N_e = 40$ elements through the half-thickness. The error value at each x/L location represents the maximum error through the thickness of the sheet at that x/L position. All simulations employ a radius $R = 257.45$ mm and $\varepsilon = 0.125$.

- [10] W. Min, Y. He, Z.-C. Sun, L.-g. Guo, X.-z. Ou, Dynamic explicit FE modeling of hot ring rolling process, *Transactions of Nonferrous Metals Society of China* 16 (2006) 1274–1280.
- [11] A. Ktari, Z. Antar, N. Haddar, K. Elleuch, Modeling and computation of the three-roller bending process of steel sheets, *Journal of mechanical science and technology* 26 (2012) 123–128.
- [12] L.-E. Lindgren, J. Edberg, Explicit versus implicit finite element formulation in simulation of rolling, *Journal of Materials Processing Technology* 24 (1990) 85–94.
- [13] J. Edberg, L.-E. Lindgren, Efficient three-dimensional model of rolling using an explicit finite-element formulation, *Communications in numerical methods in engineering* 9 (1993) 613–627.
- [14] A. Díaz, I. Cuesta, J. Alegre, A. de Jesus, J. Manso, Residual stresses in cold-formed steel members: Review of measurement methods and numerical modelling, *Thin-Walled Structures* 159 (2021) 107335.
- [15] D. Jung, D.-Y. Yang, Step-wise combined implicit–explicit finite-element simulation of autobody stamping processes, *Journal of Materials Processing Technology* 83 (1998) 245–260.
- [16] Z. Malinowski, J. Lenard, A study of the state of stress during cold striprolling, *Journal of Materials Processing Technology* 33 (1992) 273–288.
- [17] X. Shangwu, J. Rodrigues, P. Martins, Simulation of plane strain rolling through a combined finite element–boundary element approach, *Journal of Materials Processing Technology* 96 (1999) 173–181.
- [18] A. Shahani, S. Setayeshi, S. Nodamaie, M. Asadi, S. Rezaie, Prediction of influence parameters on the hot rolling process using finite element method and neural network, *Journal of materials processing technology* 209 (2009) 1920–1935.
- [19] O. Olaogun, J. Edberg, L.-E. Lindgren, O. Oluwole, E. Akinlabi, Heat transfer in cold rolling process of AA8015 alloy: a case study of 2-D FE simulation of coupled thermo-mechanical modeling, *The International Journal of Advanced Manufacturing Technology* 100 (2019) 2617–2627.
- [20] M. Safaei, W. De Waele, Towards better finite element modelling of elastic recovery in sheet metal forming of advanced high strength steel, in: *Sustainable Construction and Design 2011 (SCAD)*, volume 2, Ghent University, Laboratory Soete, 2011, pp. 217–227.
- [21] H. Qiao, M. Barnett, P. Wu, Modeling of twin formation, propagation and growth in a Mg single crystal based on crystal plasticity finite element method, *International Journal of Plasticity* 86 (2016) 70–92.
- [22] E. Q. Sun, Shear locking and hourglassing in MSC Nastran, ABAQUS, and ANSYS, in: *Msc software users meeting*, 2006, pp. 1–9.
- [23] C. D. Souto, A. Menghini, A. Diaz, J. M. Manso, A. M. de Jesus, C. A. Castiglioni, Determination of manufacturing residual stresses in cold-formed thin-walled steel profiles, *Thin-Walled Structures* 180 (2022) 109945.
- [24] H. Zhang, G. Liu, N. Guo, X. Meng, Y. Shi, H. Su, Z. Liu, B. Tang, Damage evolution of hot stamped boron steels subjected to various stress states: Macro/micro-scale experiments and simulations, *Materials* 15 (2022) 1751.
- [25] Z. Yang, X. Deng, Z. Li, Numerical modeling of dynamic frictional rolling contact with an explicit finite element method, *Tribology international* 129 (2019) 214–231.
- [26] S. Matsubara, A. Ogino, S. Nagashima, D. Okumura, Computational and physical aspects for the occurrence of crease in an elastomer under general loading conditions, *International Journal of Solids and Structures* 288 (2024) 112610.
- [27] S. Gao, J. Yang, Y. Xu, Y. Zhang, Q. Bai, Effect of dynamic constitutive differences in materials on the impact performance of cfst via secondary development of abaqus, in: *Structures*, volume 62, Elsevier, 2024, p. 106236.
- [28] X. Qian, W. Chengguo, G. Ge, The research of parallel computing for large-scale finite element model of wheel/rail rolling contact, in: *2010 3rd International Conference on Computer Science and Information Technology*, volume 1, IEEE, 2010, pp. 254–257.
- [29] F. Flanagan, D. O’Kiely, A. O’Connor, M. Erfanian, E. J. Brambley, New discoveries in cold rolling: Understanding stress distribution and parameter dependence for faster, more accurate models, in: *International Conference on the Technology of Plasticity*, Springer, 2023, pp. 211–222.